Stability of single-layer and multilayer arsenene and their mechanical and electronic properties

D. Kecik,[1] E. Durgun,[1,2,*] and S. Ciraci[3,†]

[1]*UNAM-National Nanotechnology Research Center, Bilkent University, Ankara 06800, Turkey*
[2]*Institute of Materials Science and Nanotechnology, Bilkent University, Ankara 06800, Turkey*
[3]*Department of Physics, Bilkent University, Ankara 06800, Turkey*

Using first-principles spin-polarized density functional theory, we carried out an analysis on the atomic structure, stability, energetics, and mechanical and electronic properties of single-layer structures of arsenene. These are buckled honeycomb, symmetric, and asymmetric washboard arsenene structures. Our analysis is extended to include layered three-dimensional crystalline phase of arsenic, as well as bilayer and trilayer structures to reveal dimensionality effects. The buckled honeycomb and symmetric washboard structures are shown to maintain their stability at high temperatures even when they are freestanding. As a manifestation of the confinement effect, the large fundamental band gap of single-layer phases decreases with increasing number of layers and eventually is closed. Concomitantly, lattice constants partially increase, while interlayer distances decrease. The effects of hybrid functional or self-energy corrections together with the spin-orbit coupling on the electronic structure of arsenene are crucial. The responses of direct and indirect band gaps to biaxial or uniaxial strain are rather complex and directional; while the fundamental band gap decreases and changes from indirect to direct with the biaxial strain applied to buckled arsenene, these effects are strongly directional for washboard arsenene. The width and the indirect/direct character of the band gap can be tuned by the number of layers, as well as by applied uniaxial/biaxial strain.

I. INTRODUCTION

Experimental and theoretical studies on very thin films and single-layer structures of black and blue phosphorus [1] have initiated the search for similar structures in other group V elements or pnictogens. Recent theoretical studies have predicted that nitrogen [2], phosphorus [3], arsenic [4], antimony [5–7], and bismuth [8] can form similar single-layer, buckled honeycomb, or washboard structures. Notably, phosphorus, arsenic, antimony, and bismuth have stable three-dimensional (3D) layered crystal structures, which corroborate efforts to synthesize single-layer or very thin films (or multilayers) of these elements. Recently, Kamal and Ezawa [4], based on density functional theory (DFT) [9], achieved to optimize single layers of the buckled honeycomb (*b*-As), as well as of the symmetric washboard (*w*-As) structures of arsenic, named as arsenene. They also showed that these structures are stable against the long-wavelength displacements indicating the stability at $T = 0$ K. The predicted semiconducting character having a band gap in the range of 1.5–2.10 eV and other properties of arsenene have attracted considerable interest. Very recently, various theoretical studies contributed for better understanding of arsenene [10–16]. Promising progress towards the synthesis of these phases has also been reported [17].

In this paper, starting from layered 3D crystalline phase of arsenic, i.e., gray arsenic, we performed an extensive study on mechanical and electronic properties of freestanding, single-layer (SL), bilayer (BL), and trilayer (TL) structures of arsenene and revealed the dimensionality effects. Additionally, we performed an analysis of the effects of strain on the electronic structure. In particular, for a wide range of applied

strain, we determined the strain-induced, direct-indirect transitions of the fundamental band gap together with their position in the momentum space. We, however, first clarified the following critical questions which were not treated satisfactorily yet: (i) Further to their $T = 0$ K stabilities, can arsenene structures remain stable at high temperature to sustain room-temperature applications? The answer to this question is most essential for the future applications of arsenene in two-dimensional (2D) electronics. (ii) Is SL, stable washboard structure of arsenic symmetric like phosphorene or antisymmetric like antimonene? (iii) Knowing the fact that band gaps are underestimated by standard DFT, can electronic structure calculations carried out so far, in particular the values of fundamental band gaps obtained thereof, reflect the actual situation? What are the effects of the corrections plus spin-orbit coupling applied to standard DFT results on the electronic properties of the bulk and 2D phases? This paper is unique in analyzing the low- and high-temperature stability and energetics of arsenene phases and in treating several features related to their mechanical and electronic properties consistently with the same set of parameters. The strain and layer dependent optical properties of arsenene phases are also examined in a follow-up work [18].

II. COMPUTATIONAL METHODOLOGY

Optimized atomic structure, energetics, and electronic structures are calculated by first-principles plane-wave method within spin-polarized DFT. The projector-augmented wave potentials (PAW) formalism [19,20] implemented in the Vienna *ab initio* simulation package (VASP) [21–24] is used. The electron exchange and correlation potential was described by the Perdew-Burke-Ernzerhof (PBE) form within the generalized gradient approximation (GGA) [25,26]. In addition, the van der Waals interactions were taken into account for

―――――――
*durgun@unam.bilkent.edu.tr
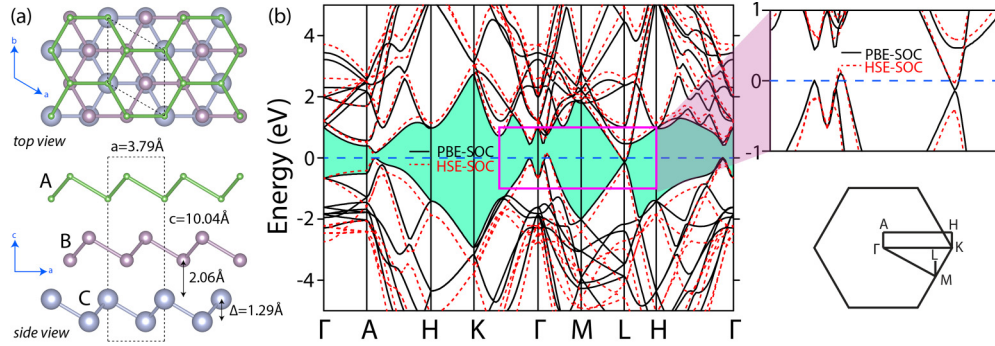†ciraci@fen.bilkent.edu.tr

FIG. 1. The atomic and electronic structure of layered, 3D gray arsenic crystal: (a) Top and side views of the optimized atomic structure. In order to show the stacking sequence, arsenic atoms in A, B, and C layers are shown by balls of different sizes. Hexagonal primitive unit cell together with lattice constants are delineated by dashed lines. (b) Electronic energy bands calculated by PBE-SOC and HSE-SOC are shown with solid and dashed lines, respectively. Zero of energy is set at the Fermi level. An expanded view of the negative indirect band gap is shown by inset on the right-hand side. The Brillouin zone underneath shows the relevant symmetry directions.

the layered structures [27,28]. The plane-wave basis set was used with an energy cutoff of 500 eV for all calculations. The structures are optimized using the conjugate gradient method, where the total energy and atomic forces are minimized. The energy difference between the sequential steps is set to 10^{-5} eV for convergence; the maximum allowed force on each atom is taken as 0.05 eV/Å. Γ-centered $47 \times 47 \times 1$ and $35 \times 35 \times 1$ grids were used for Brillouin zone (BZ) integrations of the primitive unit cell of b-As and w-As, respectively. In order to avoid spurious interactions between the periodic images, a supercell with minimum ~ 18 Å vacuum space was adopted.

The cohesive energy of b-As (w-As) is calculated from the expression $E_c = E_T[\text{As}] - E_T[\text{b-As(w-As)}]$ (per atom) in terms of the total energy of the free As atom and the optimized total energy of SL b-As (w-As) phase. Positive value of E_c implies the attractive interaction. The higher the positive E_c, the stronger is the binding. By subtracting the E_c of 3D gray As crystal from the calculated E_c of b-As (w-As), the formation energy E_f of b-As (w-As) at $T = 0$ K is calculated. A negative value of E_f implies that the formation of the given arsenene phase is energetically less favorable than the 3D bulk phase.

In addition to *ab initio* phonon calculations [29,30], the stability of the structures was tested at high temperatures by *ab initio* molecular dynamics (MD) calculations, where the velocities of atoms are rescaled at a given temperature through Verlet algorithm with time step of 1 fs.

Subsequent to the DFT results, hybrid functionals (HSE) [31–33] and the quasiparticle (QP) G_0W_0 approach [(QP)G_0W_0] [34–36], where G and W are iterated once, were used in order to obtain the corrected band structures of b-As and w-As. The effects of spin-orbit coupling (SOC) on the electronic structure are analyzed by including it to the PBE and HSE calculations.

III. GRAY ARSENIC, LAYERED 3D BULK CRYSTAL

Gray arsenic is a 3D crystalline allotrope of arsenic which has layered structure similar to layered 3D phosphorus, antimony, and bismuth. It consists of 2D buckled honeycomb layers with ABCABC... stacking along the perpendicular direction. In each layer, three alternating As atoms at the corners of the hexagon are raised: the remaining three are

lowered forming two atomic planes of As atoms with a spacing of $\Delta = 1.29$ Å. Gray arsenic has hexagonal lattice with $R - 3m$ space group. Optimized atomic structure together with optimized primitive unit cell, lattice constants, and other relevant structural parameters are described in Fig. 1(a). Buckled honeycomb layers with the minimum spacing of 2.06 Å between adjacent atomic planes suggest that arsenic can have stable 2D structures, namely, single layer or multiple layers forming very thin films.

In Fig. 1(b), we present the electronic energy band structure of gray arsenic calculated by PBE-SOC and HSE-SOC. Although it went unnoticed so far, this band structure displays interesting similarities to those of 3D layered crystals of Sb and Bi [5,8,37]. Both PBE and HSE calculations including SOC predict that 3D gray arsenic is a semimetal with a negative indirect band gap $E_{g-i} < 0$. The band gap near the Fermi level is highlighted for comparison with those of 3D layered crystals of group V elements. The E_{g-d} at L point of BZ has a small gap of 400 meV predicted by HSE-SOC (negligibly small predicted by PBE-SOC), nevertheless, E_{g-i} between the maximum of the valence band occurring along $\Gamma - M$ and minimum of conduction band at the L point is closed and has a negative value of -125 meV according to HSE-SOC (-130 meV PBE-SOC) calculations. In a recent study, it has been found out that the semimetallic properties of layered 3D As can be altered by applying moderate tensile strain [10]. The optimized atomic structure, energetics, and electronic structure discussed in this section will serve us as reference in our study of SL b-As, w-As, and their BL and TL structures.

IV. SINGLE-LAYER ARSENENE PHASES

SL arsenene phases attracted interest due to their semiconducting properties having fundamental band gaps suitable for the emerging 2D electronics. The atomic configurations and relevant structural constants of two well-known phases of SL arsenene, i.e., b-As and w-As, are described in Fig. 2. The b-As has buckled honeycomb structure like the layers of gray arsenic. As discussed earlier related with the structure of SL silicene, planar honeycomb structure is unstable due to weak π-π orbital coupling between the nearest atoms, yet is stabilized by sp^3-like hybridization of s and p orbitals upon
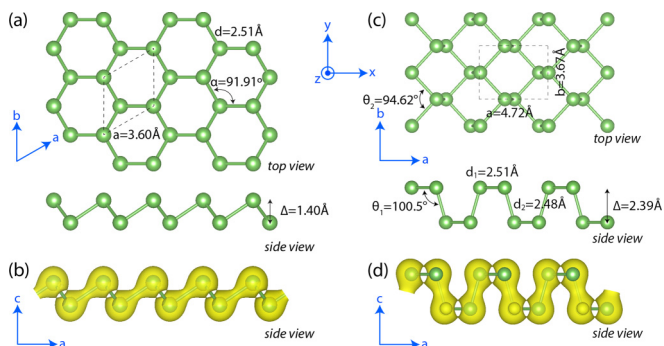
FIG. 2. The atomic structures of two SL arsenene structures: (a) top and side views of buckled honeycomb structure b-As with its 2D hexagonal lattice. a and b axes are parallel to the 2D hexagonal lattice vectors **a** and **b**. (b) Isosurfaces of the total charge density. (c) Washboard structure w-As with 2D rectangular lattice. $x \| \mathbf{a}$ lattice vector and $y \| \mathbf{b}$ lattice vector. (d) Corresponding isosurfaces of the total charge density. Primitive unit cells are delineated by dashed lines and lattice constants a, b and buckling parameter Δ, as well as relevant bond angles are indicated.

dehybridization of planar sp^2 through buckling [38–40]. The symmetric washboard structure of arsenene w-As is similar to the structure of black phosphorous; it is symmetric and consists of two atomic planes. Accordingly, it has in-plane As-As bonds (d_1) and interplane As-As bonds (d_2). Notably, the SL symmetric washboard structure of antimonene (w-Sb) was found to transform to an asymmetric washboard structure (aw-Sb) where planar Sb-Sb bonds are tilted and hence the total energy is lowered where four atomic planes in a single layer are formed [5]. A similar situation has occurred also in SL symmetric washboard structure bismuthene (w-Bi), that changes into asymmetric washboard structure (aw-Bi) [8]. In the present case, such a transition from SL symmetric to asymmetric washboard structure of arsenene did not occur. Conversely, an asymmetric washboard structure of arsenene has transformed to the symmetric one. Nevertheless, we further discuss aw-As structure in the next section.

A. Optimized structure and energetics

Two SL structures are optimized within PBE; their cohesive energies indicate that w-As has slightly stronger binding. While both binding energies are positive, the formation energies relative to 3D gray arsenic structure (i.e., free energies at $T = 0$ K) are negative and indicate that both SL structures may correspond to local minima in the Born-Oppenheimer surface. This situation necessitates a stringent test of stability performed in the next section. Upon optimization with PBE, the asymmetric washboard structure aw-As underwent a structural transition to change to the symmetric form, indicating the fact that aw-As is unstable. Recently, using dispersion correction method with Becke-Jonson damping (D3-BJ) [41,42], an asymmetric washboard structure of arsenene with relatively smaller lattice constant $a = 4.36$ Å has been predicted [13]. Here, we resolve the cause of this controversy by calculating the total energies of the present w-As structure and aw-As structure optimized in Ref. [13] using the D3-BJ method and present parameters of our calculation. We found that the symmetric w-As structure is energetically more favorable than the asymmetric aw-As structure reported in Ref. [13].

In view of the above analysis, we conclude that the stability of aw-As structure appears to be method and parameter specific. We therefore consider only b-As and w-As structures in this study. Calculated values of the optimized atomic structures of b-As and w-As, such as lattice constants, buckling parameters, As-As bonds, cohesive and formation energies, and elastic constants are listed in Table I. For the sake of comparison, the calculated values of their BL, TL, and 3D gray arsenic, as well as similar values obtained from the previous theoretical and experimental works are also included.

B. Stability analysis

The stability of SL arsenene phases at $T = 0$ K against small displacements, in particular against long-wavelength transversal displacements, are examined by performing *ab initio* phonon calculations using 7×7 and 6×6 supercell for b-As and w-As, respectively. Generally, the imaginary

TABLE I. Calculated values for the atomic structure, energetics, and mechanical properties of SL arsenene phases and their BL, TL, and layered 3D crystal structures: lattice constants, a and b; bond lengths d_1 and d_2; buckling, Δ; cohesive E_c and formation E_f energies; components of in-plane stiffness C_x, C_y; Poisson's ratio ν_{xy}, ν_{yx}. Interplanar distance l for BL and TL is given in parentheses, instead of Δ.

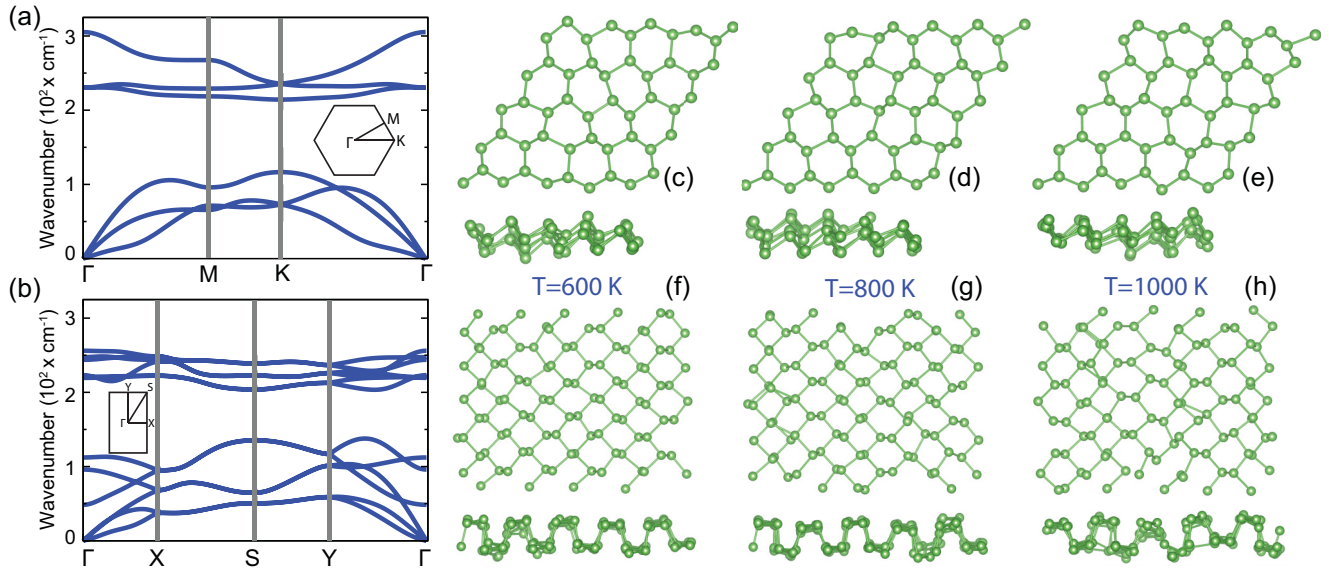| Structure	a (Å)	b (Å)	d_1 (Å)	d_2 (Å)	Δ (l) (Å)	E_c (eV)	E_f (eV)	C (N/m)	ν (%)
SL b-As	3.60	3.60	2.51		1.40	3.13	−0.12	$C = 58$	$\nu_{xy} = \nu_{yx} = 0.21$
	3.61 [4]	3.61 [4]	2.56 [4]		1.39 [4]	2.99 [4]			
SL w-As	4.72	3.67	2.51	2.48	2.39	3.13	−0.11	$C_x = 20$; $C_y = 55$	$\nu_{xy} = 0.33$; $\nu_{yx} = 0.91$
	4.77 [4]	3.68 [4]	2.50 [4]	2.48 [4]		2.95 [4]			
SL aw-As	4.77	3.68	2.50	2.48	2.42	3.13	−0.12		
	4.36 [13]	3.74 [13]	2.52 [13]	2.48 [13]	2.42 [13]				
BL b-As	3.61	3.61	2.51		(3.27)	3.18	−0.07		
			2.51 [43]		(3.14 [43])	2.85 [43]			
BL w-As	4.71	3.63	2.51	2.48	(3.23)	3.19	−0.06		
TL b-As	3.63	3.63	2.49		(3.10)	3.20	−0.05		
TL w-As	4.31	3.72	2.54	2.48	(3.01)	3.22	−0.03		
Gray As	3.79	3.79 ($c = 10.04$)			1.29	−3.25			
	3.82 [4]	3.82 ($c = 10.75$) [4]				−2.99 [4]			
	3.76 (expt.) [44]					−2.96 [45]			

FIG. 3. Calculated phonon bands: (a) SL b-As, (b) SL w-As. Brillouin zones and symmetry points are shown by insets. (c)–(e) Snapshots of atomic structure of SL b-As obtained by *ab initio* molecular dynamics calculations at $T = 600$, 800, and 1000 K, respectively. (f)–(h) Snapshots of atomic structure of SL w-As obtained by *ab initio* molecular dynamics calculations at $T = 600$, 800, and 1000 K, respectively.

frequencies in phonon calculations imply instability or structural transitions. Conversely, positive frequencies of all modes of SL b-As and w-As in their respective BZ demonstrate their stability at low temperatures. While optical and acoustical branches of b-As are well separated by a gap, the branches associated with the modes of specific atoms of w-As overlap with the acoustical modes indicating possible structural transitions at high temperature. The calculated phonon bands presented in Figs. 3(a) and 3(b) agree with previous calculations [4]. In contrast, phonon dispersions of w-As optimized within D3-BJ method resulted in imaginary frequencies near the Γ point [13]. Similar situations have also occurred when the supercell size is insufficient and disappeared upon increasing the size.

It should be noted that even if the calculated frequencies of all phonon modes are positive, it is not sufficient to decide whether SL arsenene structures will remain stable at high temperatures. If the local minima corresponding to these SL phases are not deep enough, the structures can be dissociated through thermal excitations at high temperatures. Therefore, further to the phonon calculations of the optimized atomic structures, high-temperature MD calculations are critical to demonstrate that b-As and w-As can remain stable above room temperature. This issue is crucial for the future applications of As SL or multilayer phases to operate slightly above the room temperature. In this part, we carried out finite-temperature *ab initio* MD calculations starting from 200 K, and subsequently by raising the temperature to 400, 600, and 800 K and by holding the structure for 1 ps at each of these temperatures. Finally, the temperature is raised to 1000 K, where MD simulations were carried out for 2 ps. At temperatures as high as $T = 1000$ K, these structures maintained their form, except thermally induced deformation; no bond breaking or clustering occurred. As one can depict from Figs. 3(f)–3(h), as of 600 K, in-plane As-As bonds of w-As start to tilt or buckle so that w-As undergoes a structural transformation. In compliance with the phonon dispersion, aw-As appears as a high-temperature phase of SL arsenene.

We note that the simulation time of few picoseconds appears long for computation, nevertheless, could be insufficient for the real situation. Therefore, our MD results cannot indicate that SL phases of arsenene can sustain at temperatures as high as 1000 K; they rather imply the stability at least slightly above room temperature since the statistics is speeded up at high temperature. In summary, present phonon frequency calculations together with *ab initio* MD simulations at high temperature provide strong evidences in favor of the stability of suspended SL b-As and w-As structures and suggest that they preserve their form and maintain their physical properties at least in room-temperature applications. When grown on specific substrates, the stability of SL arsenene phases can be enhanced further.

C. Elastic properties

Elastic properties are essential in the characterization of arsenene phases and provide further valuable information about their stability, strength, and elastic behaviors. For SL b-As and w-As, we carried out calculations of their in-plane stiffness $C = (1/A)\partial^2 E_T / \partial\epsilon^2$ and Poisson's ratio $\nu_{xy} = -\epsilon_y / \epsilon_x$. In-plane stiffness is a measure of the robustness of the structure. Poisson's ratio is critical for the variation of the electronic structure, in particular for possible metal-insulator transitions under tensile strain. We calculated the in-plane stiffness values of arsenene phases based on PBE. The in-plane stiffness value of b-As is homogeneous and is $C = 58$ N/m, whereas the in-plane stiffness of w-As exhibits directionality due to its structure and thus $C_x = 20$ N/m and $C_y = 55$ N/m. While the homogeneous Poisson's ratio of b-As was found as $\nu_x = 0.21$, a clear directionality for w-As was once again observed, as $\nu_{xy} = 0.33$ and $\nu_{yx} = 0.91$ owing to the large value of Δ. These calculated values of Poisson's ratio are comparable to the values of aw-As reported as $\nu_{xy} = 0.27$ and $\nu_{yx} = 1.43$ [13].
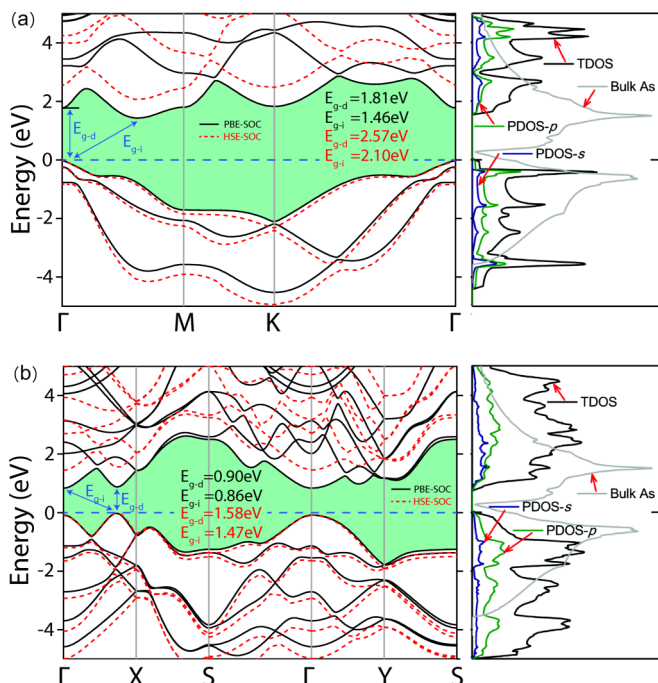
FIG. 4. Electronic energy band structures of SL arsenene phases. Bands calculated by PBE-SOC and HSE-SOC are shown by solid and dashed lines. Band gaps are shaded and direct E_{g-d} and indirect E_{g-i} band gaps are indicated by arrows. Zero of energy is set at the top of the valence band. (a) Energy bands, total densities of states (TDOS), and s-, p-orbital projected densities of states (PDOS) of b-As. TDOS of 3D gray arsenic is also shown by gray light lines for the sake of comparison. (b) Same for w-As.

V. ELECTRONIC STRUCTURE OF SINGLE-LAYER ARSENENE PHASES

In this section, we present a thorough analysis of the electronic structure of SL arsenene phases, including the effects of spin-orbit coupling, HSE and (QP)G_0W_0 corrections on the electronic states, and fundamental band gap. We then compare our results with the previous studies. The calculated electronic band structure, total (TDOS), and s- and p-orbital projected densities of states (PDOS) of b-As and w-As are presented in Figs. 4(a) and 4(b), respectively. For the sake of comparison, the total density of states of 3D gray arsenic is also included.

The indirect and direct band gaps of b-As calculated by PBE as $E_{g-i} = 1.59$ eV and $E_{g-d} = 1.94$ eV are reduced by $\sim 8\%$ upon the inclusion of SOC and become $E_{g-i} = 1.46$ eV and $E_{g-d} = 1.81$ eV. These indirect and direct band gaps are widened to $E_{g-i} = 2.10$ eV and $E_{g-d} = 2.57$ eV after the HSE correction with SOC included. Like PBE gaps, indirect and direct band gaps calculated by HSE decreases upon the inclusion of SOC. We also performed calculations for the (QP)G_0W_0 corrections, which lead the direct and indirect band gaps to further increase relative to those obtained by HSE correction: the indirect (direct) band gap of SL b-As becomes $E_{g-i} = 2.64$ eV (3.27 eV). Similarly, the indirect (direct) band gap of SL w-As is found to be $E_{g-i} = 1.58$ eV (1.83 eV).

It is noted that 3D gray arsenic, which has a 2D hexagonal lattice consisting of layers similar to that of SL b-As, but lattice constants being $\sim 4\%$ larger, is a semimetal. This situation

TABLE II. Fundamental indirect and direct band gaps of SL, BL, and TL structures of b-As, w-As, and 3D gray As calculated by PBE, PBE-SOC, HSE, HSE-SOC, and G_0W_0 in units of eV. Values given in parentheses refer to non-SOC calculations. "i" refers to indirect and "d" to direct band gaps. Previous results are also given for comparison.

Structure		E_g-PBE	E_g-HSE	E_g-G_0W_0
SL b-As	i	1.46 (1.59)	2.10 (2.25)	(2.64)
	d	1.81 (1.94)	2.57 (2.73)	(3.27)
SL w-As	i	0.86 (0.80)	1.47 (1.43)	(1.58)
	d	0.90 (0.90)	1.58 (1.48)	(1.83)
BL b-As	i	0.70	1.54	
	d	1.40	2.33	
BL w-As	i	Semimetal		
	d	Semimetal	0.33	
TL b-As	i	0.22	0.75	
	d	0.96	1.50	
TL w-As	i	Semimetal		
	d	Semimetal	Semimetal	
Gray As		Semimetal	Semimetal	
Prev. (SL b-As)		1.51 [46] (i), 1.64 [4] (i)	2.2 [43] (i)	
Prev. (SL w-As)		0.83 [4] (i), 0.79 [12] (i)		
Prev. (BL w-As)		0.47 [12] (i)		
Expt. (b-As)		2.3 [17] (i)		

indicates the crucial effects of interlayer interaction, as well as As-As bond length on the electronic structure. It is known that the smaller the bond length is, the wider is the fundamental band gap [47]. The opening of the band gap in SL b-As can also be viewed as confinement effect. In view of these predictions, we note that recently synthesized arsenene phase with measured band gap of ~ 2.3 eV [17] may be identified as b-As phase.

The effect of SOC on the band structure of w-As is complex. While indirect band gap of w-As calculated by PBE, $E_{g-i} = 0.80$ eV increases to $E_{g-i} = 0.86$ eV upon the inclusion of SOC, the direct PBE band gap $E_{g-d} = 0.90$ eV is only slightly altered. Recent calculations by Luo et $al.$ [12] predict that direct and indirect PBE band gaps decrease slightly upon the inclusion of SOC. The band gaps increase upon HSE correction to $E_{g-i} = 1.43$ eV and $E_{g-d} = 1.48$ eV when applied to PBE only, but they slightly increase to $E_{g-i} = 1.47$ eV and $E_{g-d} = 1.58$ eV upon inclusion of SOC. Similar to the buckled phase, the band gap of SL w-As further increases to $E_{g-i} = 1.58$ eV with the (QP)G_0W_0 correction.

The above analysis suggests that hybrid functional or self-energy corrections of electronic energies appear to be necessary for the realistic treatment of the electronic and optical properties. The electronic structures of arsenene phases with corrected band gaps show their crucial potential in the emerging field of 2D electronics. A summary of the calculated fundamental band gaps of SL b-As and w-As together with present results for BL and TL arsenenes and previous works are presented in Table II.

Effects of biaxial and uniaxial strain

Compared to 2D thin films and 3D bulk crystal, SL arsenene structures can sustain relatively larger uniaxial strains (ϵ). Larger strains, in turn, can lead to significant effects on the
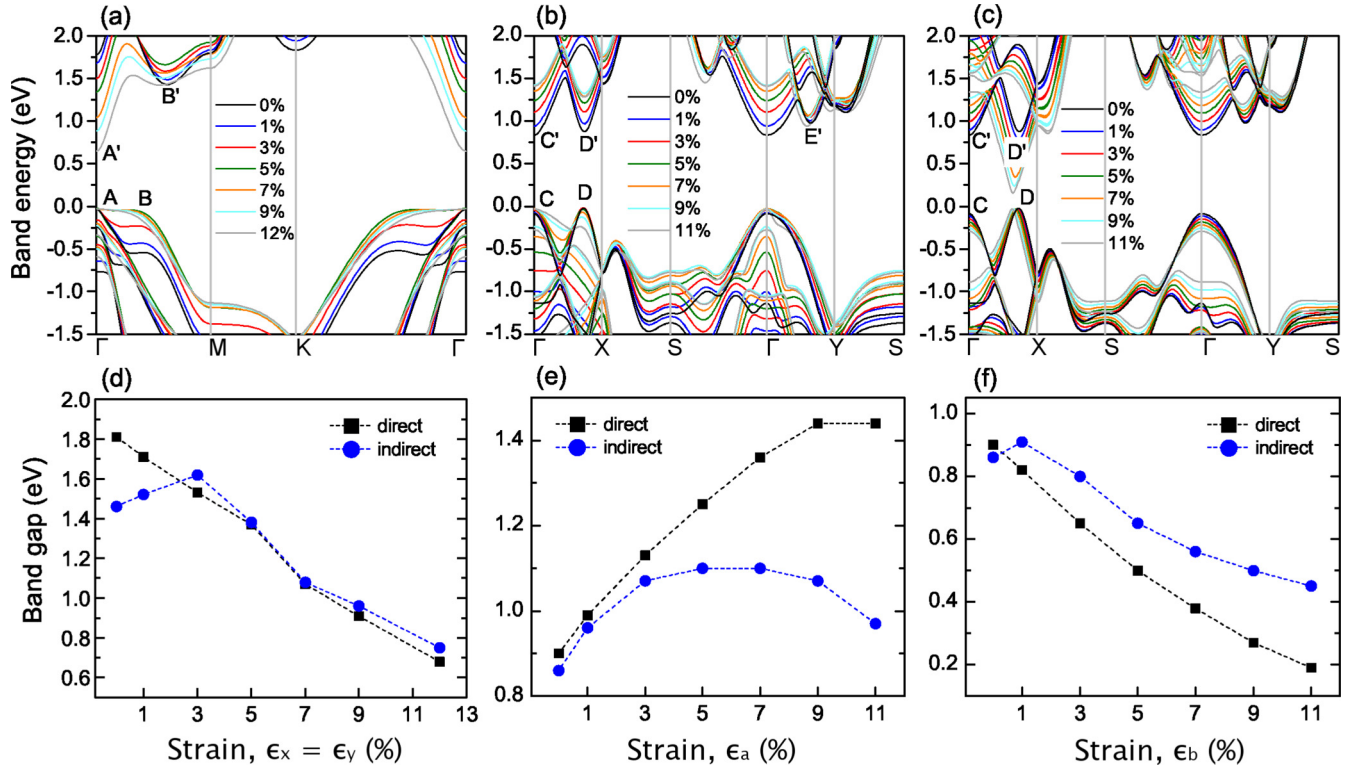
FIG. 5. The band structures and variation of the direct E_{g-d} and indirect E_{g-i} band gaps of SL arsenene structures under applied tensile strain ϵ calculated using PBE-SOC: (a) Variation of the band structure of b-As with the biaxial tensile strain ϵ applied along the directions of 2D hexagonal lattice vectors. (b) Variation of the band structure of w-As with the uniaxial tensile strain ϵ, applied along lattice vector **a**. (c) Variation of the band structure of w-As with the uniaxial tensile strain ϵ, applied along lattice vector **b**. Critical band points at the highest valence and the lowest conduction bands, between which the direct and indirect band gaps can occur are marked as A, A', etc. (d) Variation of E_{g-d} and E_{g-i} of b-As with biaxial strain described in (a). (e) Variation of E_{g-d} and E_{g-i} of w-As with uniaxial strain $\epsilon\|$**a**. (f) Same as (e) for $\epsilon\|$**b**.

electronic structure. In many of the SL structures, the response of the bands near the fundamental band gap can be different. While specific bands originating from bonding states can rise, some bands are lowered with applied uniaxial strain. Moreover, in the strain-induced variation of the electronic structure, the direction of the uniaxial strain can matter. In this section, we discuss the variation of the width and the character of the indirect or direct band gaps of SL b-As and w-As calculated using PBE-SOC. Earlier, the effect of strain has been studied within DFT in Refs. [4,7,12–15] in different phases of SL. Analysis by Kamal and Ezawa [4] comprised both compressive and tensile strains. Luo *et al.* [12] considered also variation of effective mass with strain. Here, we examined the effects of strain from a different point of view: the positions of the direct and indirect band gaps in momentum space are determined as a function of strain. Additionally, tuning of the direct-indirect band gap and metal-insulator transitions with strain are studied. We consider tensile strains up to $\epsilon \simeq 12\%$; at higher strain levels, a rigorous test of stability is needed.

In Figs. 5(a)–5(c), we present the strain-induced variations of the energy bands around the fundamental band gap of SL b-As and w-As along the selected symmetry directions of BZ. Under the biaxial strain, which are applied along **a** and **b** lattice vectors of 2D hexagonal lattice simultaneously, b-As expands uniformly maintaining the buckled honeycomb

structure. Specific band points in Figs. 5(a)–5(c) are indicated as A, B, etc., which are critical for setting direct and indirect band gaps for different values of strains. Figures 5(d)–5(f) show the variation of the direct and indirect band gaps with strain.

In SL b-As, E_{g-d} occurs $A \to A'$ for $0 < \epsilon < 12\%$, but E_{g-i} occurs between different **k** points with varying ϵ. E_{g-i} occurs between $A \to B'$ for $1\% < \epsilon < 3\%$; $B \to A'$ for $5\% < \epsilon < 12\%$. In Fig. 5(d), the smallest fundamental band gap occurs as E_{g-i} for $\epsilon \leqslant 2\%$, but switches to be direct E_{g-d} for $2\% < \epsilon$. We calculated the direct band gap $E_{g-d} = 0.68$ eV and the indirect band gap $E_{g-i} = 0.75$ eV for $\epsilon = 12\%$ within PBE-SOC. Apparently, the negative band gap revealed by Zhang *et al.* [14] in PBE calculation at $\epsilon = 12\%$, which is taken as the indication of quantum spin Hall effect, did not occur.

SL w-As can sustain relatively larger strains and the variation of its gap displays a directional behavior different from SL b-As. In SL w-As, when $\epsilon\|$**a** lattice vector as in Figs. 5(b) and 5(e), $E_{g-i} < E_{g-d}$ for $0 < \epsilon < 11\%$, the fundamental gap first increases, then passes through a maximum and decreases to a value larger than that of $\epsilon = 0$, i.e., $E_{g-i} = 0.90$ eV. While the direct gap occurs as $D \to D'$ for $0 < \epsilon < 11\%$, indirect gap is first between $D \to C'$ for $\epsilon \leqslant 1\%$, then it becomes between $D \to E'$ for $1\% < \epsilon < 3\%$, finally it switches between $C \to E'$ for $5\% < \epsilon < 11\%$.

However, when uniaxial strain $\epsilon \| \mathbf{b}$ lattice vector as in Figs. 5(c) and 5(f), initially $E_{g-i} < E_{g-d}$ for $\epsilon \lesssim 0.75\%$, but for $0.75\% < \epsilon \leqslant 11\%$ the character of the fundamental band gap changes and it becomes direct. All direct transitions occur between $D \rightarrow D'$ and all indirect transitions between $C \rightarrow D'$ in the range of applied strain considered in this study. Moreover, the fundamental band gap decreases with increasing strain. Eventually, the smallest band gap decreases from 0.86 to 0.20 eV at $\epsilon = 11\%$. This situation can suggest that for $\epsilon > 11\%$ applied along the $\mathbf{b}$-lattice vector, the w-As phase can be metallized.

Apparently, the width and character of the fundamental band gaps of two SL arsenene structures display dramatic changes with the direction, as well as the magnitude of the applied strain. In particular, the direct-indirect transition with the applied strain may lead to crucial consequences. These unusual behaviors, which can be tuned by biaxial and uniaxial strain, can be utilized for photovoltaic and possible laser applications.

VI. BILAYER AND TRILAYER ARSENENE

BL and TL of b-As and w-As are important since their properties are expected to differ from those of SL phases. Second, BL structures are the first steps towards the formation of multilayer structures and layered 3D bulk crystal. The variation of physical properties, in particular the changes in the width and type of the fundamental band gap with the number of layers, is prominent for technological applications. Based
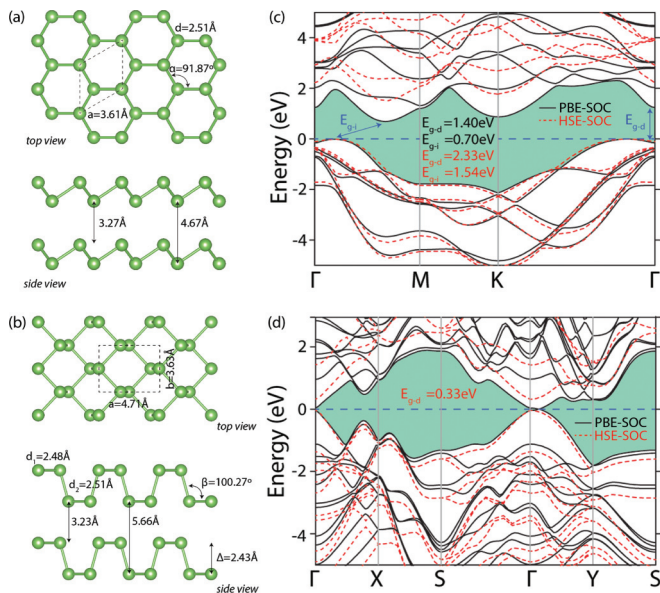

FIG. 6. The atomic and electronic structures of bilayer (BL) arsenene phases: (a) Top and side views of BL b-As with AA minimum energy stacking and relevant structural parameters. (b) Top and side views of the atomic structure of BL w-As with AA minimum energy stacking. (c) Corresponding energy band structure calculated by PBE-SOC (solid lines) and HSE-SOC (dashed lines) of BL b-As. (d) Corresponding energy band structure of BL w-As. The band gaps between conduction and valence bands are shaded, and direct and indirect band gaps are indicated by arrows. The zero of the band energy is set at the top of the valence band.
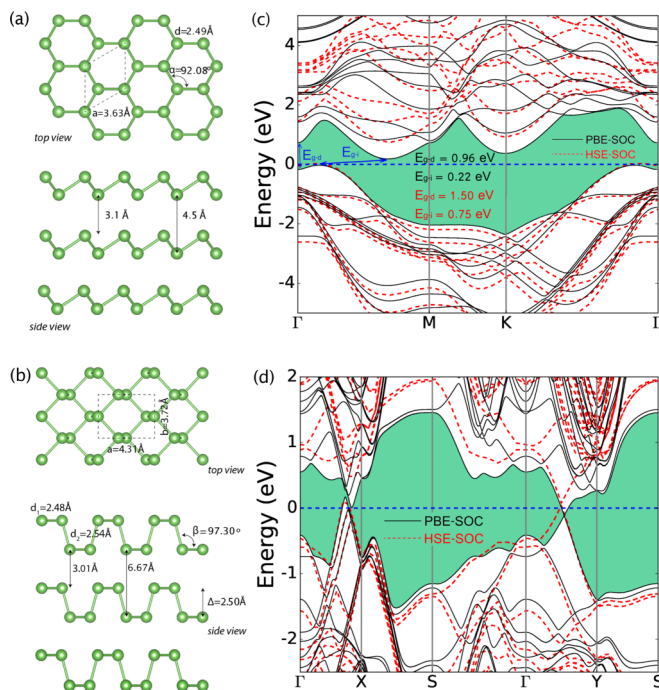

FIG. 7. The atomic and electronic structures of trilayer (TL) arsenene phases: (a) Top and side views of TL b-As with AAA minimum energy stacking and relevant structural parameters. (b) Top and side views of the atomic structure of TL w-As with AAA minimum energy stacking. (c) Corresponding energy band structure calculated by PBE-SOC (solid lines) and HSE-SOC (dashed lines) of TL b-As. (d) Corresponding energy band structure of TL w-As. The band gaps between conduction and valence bands are shaded, and direct and indirect band gaps are indicated by arrows. The zero of the band energy is set at the top of the valence band.

on DFT calculations, Luo *et al.* [12] investigated the shifts of the band edges of w-As and reported a monotonic decrease of band gap with increasing number of layers $1 \geqslant n \geqslant 4$. It is therefore interesting to know how the electronic properties can change by going from SL to BL and TL of b- and w-As in order to understand multilayers. Having discussed gray arsenic in Sec. III, the dimensionality effects regarding b-As can also be revealed.

In Figs. 6 and 7, we show the atomic and electronic structures of BL and TL of b-As and w-As phases. The energetics and structural parameters related with BL and TL are summarized in Table I, which can be compared with the values calculated for SL, as well as for 3D gray arsenic. In Table II, the calculated values regarding the electronic structure, in particular direct and indirect band gaps, are presented.

For BL of b-As, the AA stacking corresponds to minimum total energy and is energetically more favorable by 51 meV relative to the AB stacking. By going from SL to BL, both indirect and direct band gaps of BL b-As decrease. However, the decrease of the indirect band gap is more pronounced than that of the direct band gap. This situation can be understood by the fact that the energy difference between the bonding and antibonding As-As states, wherefrom the edges of conduction and valence bands originate, is large [47]. Here, we note that

the spacing between the nearest atomic planes is 3.27 Å, which is 1.21 Å larger than the corresponding spacing in 3D gray arsenic. Therefore, the interlayer interaction in BL is lower than that in 3D gray arsenic. This explains why BL continues to be a semiconductor and is reminiscent of SL structure.

For BL of w-As, the AA stacking is favorable by 23 meV relative to the AB stacking. Its smallest spacing between As atomic planes is 3.23 Å and indicates also weak coupling between the layers. Although BL w-As is predicted to be metallic with PBE-SOC calculation, a direct band gap of 0.33 eV is opened up after HSE-SOC correction, making it also a semiconductor. Notably, the fundamental band gap changes to direct from indirect in BL w-As. In contrast, Luo *et al.* [12] found a direct band gap of 0.47 eV in PBE-SOC calculations.

Similar to BL, in TL b-As the AAA stacking is favorable by 43 meV relative to the ABA stacking where As-As bonds in different buckled hexagons are staggered similar to the diamond structure. The lattice constant is slightly enlarged relative to SL and BL b-As. The band gap is indirect and $E_{g-i} = 0.22$ eV within PBE-SOC; it is $\sim\frac{1}{6}$ of that of SL b-As and $\sim\frac{1}{3}$ of BL b-As. However, with HSE-SOC correction, the fundamental band gap is widened to 0.75 eV. It is demonstrated that owing to the confinement effect, as the number of layers n increases, the band gap decreases. On the other hand, the interlayer spacing is smaller than that of BL b-As, indicating slightly stronger interlayer interaction. This situation suggests that the band gap of very thin b-As films can be tuned by the number of layers. Eventually, as $n \to \infty$, the thin film approaches to semimetallic 3D gray arsenic. As for the TL w-As, its AAA stacking is also more favorable by 108 meV relative to the ABA stacking. However, the fundamental band gap is closed and TL structure becomes a semimetal according to PBE-SOC calculations. Upon HSE-SOC correction, the semimetallic character is preserved. Notably, PBE-SOC calculations of Luo *et al.* [12] predict a direct band gap of 0.30 eV for TL w-As.

VII. CONCLUSIONS

A layered 3D crystal of arsenic, named as gray arsenic, is a semimetal with slightly overlapping conduction and valence bands. The dispersion of these bands at the edges of the fundamental gap is rather complex and reminiscent of the same bands of 3D Sb and Bi. The interlayer interaction is significant and gives rise to the formation of semimetal from the individual layers which, in turn, are wide-band-gap semiconductors when they are freestanding.

Freestanding, single-layer arsenene phases are shown to maintain their stability at least at room temperature and above it. Our analysis indicates that the asymmetric washboard structure is not favored at low temperature unlike antimonene, but symmetric washboard structure is expected to transform to asymmetric one at high temperature. These single-layer structures have fundamental band gaps in the energy range which are suitable for 2D optoelectronic applications at room temperature. Additionally, the width of the band gap, as well as the direct/indirect character can be tuned by the number of layers and by applied biaxial and uniaxial strain. The indirect band gap of single layer of buckled arsenene is reduced by $\sim\frac{1}{2}$ in the bilayer structure and $\sim\frac{1}{6}$ in trilayer. Biaxial and uniaxial strains induce crucial changes in the electronic structure of single-layer arsenene. Depending on the applied strain, the character and the width of the fundamental (lowest) band gap between the minimum of conduction and maximum of valence band, as well as the momentum of these band extrema, undergo changes. All these effects of strain are revealed and given in detail. Uniaxial strain parallel to the long edge of the rectangular primitive unit cell causes the fundamental band gap to decrease and perhaps eventually to close, leading to a metal-insulator transition. The extended analysis on strain and layer dependent optical properties of arsenene phases including excitonic effects can be found in a follow-up work [18].

[1] L. Li, Y. Yu, G. J. Ye, Q. Ge, X. Ou, H. Wu, D. Feng, X. H. Chen, and Y. Zhang, Nat. Nanotechnol. **9**, 372 (2014).

[2] V. O. Ozçelik, O. Ü. Aktürk, E. Durgun, and S. Ciraci, Phys. Rev. B **92**, 125420 (2015).

[3] Z. Zhu and D. Tomanek, Phys. Rev. Lett. **112**, 176802 (2014).

[4] C. Kamal and M. Ezawa, Phys. Rev. B **91**, 085423 (2015).

[5] O. Ü. Aktürk, V. O. Ozçelik, and S. Ciraci, Phys. Rev. B **91**, 235446 (2015).

[6] O. Ü. Aktürk, E. Aktürk, and S. Ciraci, Phys. Rev. B **93**, 035450 (2016).

[7] S. Zhang, Z. Yan, Y. Li, Z. Chen, and H. Zeng, Angew. Chem., Int. Ed. Engl. **54**, 3112 (2015).

[8] E. Aktürk, O. Ü. Aktürk, and S. Ciraci, Phys. Rev. B **94**, 014115 (2016).

[9] W. Kohn and L. J. Sham, Phys. Rev. **140**, A1133 (1965).

[10] Z. Zhu, J. Guan, and D. Tomanek, Phys. Rev. B **91**, 161404 (2015).

[11] L. Kou, Y. Ma, X. Tan, T. Frauenheim, A. Du, and S. Smith, J. Phys. Chem. C **119**, 6918 (2015).

[12] K. Luo, S. Y. Chen, and C. G. Duan, Sci. China-Phys. Mech. Astron. **58**, 087301 (2015).

[13] Y. Wang and Y. Ding, J. Phys.: Condens. Matter **27**, 225304 (2015).

[14] H. Zhang, Y. Ma, and Z. Chen, Nanoscale **7**, 19152 (2015).

[15] C. Wang, Q. Xia, Y. Nie, M. Rahman, and G. Guo, AIP Adv. **6**, 035204 (2016).

[16] F. Ersan, E. Aktürk, and S. Ciraci, J. Phys. Chem. C **120**, 14345 (2016).

[17] H. S. Tsai, S. W. Wang, C. H. Hsiao, C. W. Chen, H. Ouyang, Y. L. Chueh, H. C. Kuo, and J. H. Liang, Chem. Mater. **28**, 425 (2016).

[18] D. Kecik, E. Durgun, and S. Ciraci, Succeeding paper Phys. Rev. B **94**, 205410 (2016).

[19] P. E. Blöchl, Phys. Rev. B **50**, 17953 (1994).

[20] M. Gajdoš, K. Hummer, G. Kresse, J. Furthmüller, and F. Bechstedt, Phys. Rev. B **73**, 045112 (2006).

[21] G. Kresse and J. Hafner, Phys. Rev. B **47**, 558 (1993).

[22] G. Kresse and J. Hafner, Phys. Rev. B **49**, 14251 (1994).

[23] G. Kresse and J. Furthmüller, Comput. Mater. Sci. **6**, 15 (1996).

[24] G. Kresse and J. Furthmüller, Phys. Rev. B **54**, 11169 (1996).

[25] J. P. Perdew, K. Burke, and M. Ernzerhof, Phys. Rev. Lett. **77**, 3865 (1996).

[26] J. P. Perdew, K. Burke, and M. Ernzerhof, Phys. Rev. Lett. **78**, 1396 (1997).

[27] S. J. Grimme, Comput. Chem. **27**, 1787 (2006).

[28] T. Bucko, J. Hafner, S. Lebegue, and J. G. Angyan, J. Phys. Chem. A **114**, 11814 (2010).

[29] D. Alfe, Comput. Phys. Commun. **180**, 2622 (2009).

[30] S. Baroni, S. de Gironcoli, A. Dal Corso, and P. Giannozzi, Rev. Mod. Phys. **73**, 515 (2001).

[31] J. Paier, M. Marsman, K. Hummer, G. Kresse, I. C. Gerber, and J. G. Angyan, J. Chem. Phys. **124**, 154709 (2006).

[32] J. Heyd, G. E. Scuseria, and M. Ernzerhof, J. Chem. Phys. **118**, 8207 (2003); **124**, 219906 (2006).

[33] J. Heyd and G. E. Scuseria, J. Chem. Phys. **120**, 7274 (2004); **121**, 1187 (2004).

[34] L. Hedin, Phys. Rev. **139**, A796 (1965).

[35] M. S. Hybertsen and S. G. Louie, Phys. Rev. B **34**, 5390 (1986).

[36] M. Shishkin and G. Kresse, Phys. Rev. B **74**, 035101 (2006).

[37] I. Aguilera, C. Friedrich, and S. Blügel, Phys. Rev. B **91**, 125129 (2015).

[38] E. Durgun, S. Tongay, and S. Ciraci, Phys. Rev. B **72**, 075420 (2005).

[39] S. Cahangirov, M. Topsakal, E. Aktürk, H. Sahin, and S. Ciraci, Phys. Rev. Lett. **102**, 236804 (2009).

[40] S. Cahangirov, M. Topsakal, and S. Ciraci, Phys. Rev. B **81**, 195120 (2010).

[41] S. Grimme, J. Antony, S. Ehrlich, and K. Krieg, J. Chem. Phys. **132**, 154104 (2010).

[42] S. Grimme, S. Ehrlich, and L. Goerigk, J. Comput. Chem. **32**, 1456 (2011).

[43] H. Cao, Z. Yu, and P. Lu, Superlattices Microstruct. **86**, 501 (2015).

[44] D. Schiferl and C. S. Barrett, J. Appl. Crystallogr. **2**, 30 (1969).

[45] C. Kittel, *Introduction to Solid State Physics*, 8th ed. (Wiley, Hoboken, NJ, 2004).

[46] Y. D. Wang and Y. Ding, Phys. Chem. Chem. Phys. **17**, 27769 (2015).

[47] W. A. Harrison and S. Ciraci, Phys. Rev. B **10**, 1516 (1974); S. Ciraci, I. P. Batra, and W. A. Tiller, *ibid.* **12**, 5811 (1975).